A VIRTUAL REPRESENTATION FOR TIME- AND FREQUENCY-SELECTIVE CORRELATED MIMO CHANNELS

Akbar M. Sayeed

Electrical and Computer Engineering
University of Wisconsin-Madison

ABSTRACT

A key to reliable communication is a fundamental understanding of the interaction between the signal space and the channel. In time- and frequency-selective MIMO (space-time) fading channels this interaction happens in time, frequency and space. In this paper we propose a four-dimensional Karhunen-Loeve-like virtual representation for space-time channels that captures the essence of such interaction and exposes the intrinsic degrees of freedom in the channel. The four dimensions are: time, frequency and the two spatial dimensions at the transmitter and receiver. The key signal space parameters are the signaling duration, bandwidth and the two array apertures. The corresponding channel parameters are the delay, Doppler and the two angular spreads associated with the scattering environment. The representation induces a virtual partitioning of propagation paths in time, frequency and space that reveals their contribution to channel capacity and diversity. It also exposes fundamental dependencies between time, frequency and space thereby revealing the essential degrees of freedom.

1. INTRODUCTION

The capacity and diversity afforded by a time- and frequency-selective MIMO (space-time) fading channel is due to the distribution of scatterers in space and the relative motion of the transmitter and receiver arrays. The distribution of scatterers and antenna array parameters determine the statistics of the space-time channel, which in turn determine its capacity and diversity. Accurate modeling of the scattering environment is thus paramount to realizing the full potential of antenna arrays. A key to reliable communication is a fundamental understanding of interaction between the channel and the signal space. An *effective channel representation* that captures the essence of such interaction is all this is needed from a communication viewpoint. In space-time channels, this interaction happens in four signal space dimensions: time, frequency, and the spatial dimensions at the transmitter and receiver.

In this paper, we propose a new virtual representation for space-time channels that captures the essence of channel-signal space interaction in time, frequency and space. It is a generalization of the virtual representation for narrowband correlated MIMO channels introduced in [1]. Each physical scatterer can be associated with a unique Angle of Departure (AoD), Angle of Arrival (AoA), delay, and Doppler shift. The virtual representation replaces the actual physical scatterers with virtual scatterers associated with fixed uniformly spaced AoD's, AoA's, delays and Doppler shifts on a four-dimensional (4D) grid. The grid spacings in the four dimensions correspond to the resolutions in time, frequency and the two spatial dimensions that are determined by the signaling bandwidth, duration, and array apertures, respectively. The virtual representation is a 4D Fourier series for the time-varying frequency response channel matrix, $\boldsymbol{H}(t,f)$, and yields many powerful insights. First, under the assumption of uncorrelated scattering, we show that $\boldsymbol{H}(t,f)$ is a segment of a 4D wide-sense stationary (WSS) process and the virtual representation coefficients constitute the corresponding uncorrelated spectral representation. Thus, the virtual representation captures the essential degrees of freedom in the channel in temporal, spectral and spatial dimensions that in turn determine its statistics, capacity and diversity. Second, via the concept of virtual scatterers, the virtual representation also yields a simple and intuitively appealing interpretation of the scattering environment and its effects on capacity [1]. Finally, the representation induces a virtual partitioning of propagation paths that explicitly reveals their contribution to channel capacity and diversity. In particular, it unravels fundamental dependencies in time, frequency and space that enable accurate estimates of channel capacity and diversity.

The next section presents a general model for space-time channels. Section 3 introduces the virtual representation, including the virtual path partitioning and its implications for channel statistics. Section 4 discusses fundamental dependencies between time, frequency and space. Section 5 shows some numerical results that confirm the insights afforded by the virtual framework.

2. A GENERAL MODEL FOR SPACE-TIME CHANNELS

Consider a transmitter array with P elements and a receiver array with Q elements. We are interested in representing the space-time channel over a signaling duration T and two-sided bandwidth W. In the absence of noise, the channel equation is

$$\boldsymbol{x}(t) = \int_{-W/2}^{W/2} \boldsymbol{H}(t,f)\boldsymbol{S}(f)e^{j2\pi ft}df, \;\; 0 \le t \le T, \qquad (1)$$

where $\boldsymbol{s}(t)$ is the P-dimensional transmitted signal, $\boldsymbol{S}(f)$ is the Fourier transform of $s(t)$, $\boldsymbol{x}(t)$ is the Q-dimensional received signal, and $\boldsymbol{H}(t,f)$ denotes the *time-varying frequency response matrix* coupling the transmitter and receiver elements. We index entries of $\boldsymbol{H}(t,f)$ as $H(i,k;t,f) \;:\; i = 0,1,\cdots,Q-1,\; k = 0,1,\cdots,P-1$.

We focus on one-dimensional ULAs of antennas at the transmitter and receiver and consider far-field scattering characteristics. Let d_T and d_R denote the antenna spacings at the transmitter and

This research was supported in part by the National Science Foundation under grants CCR-9875805 and CCR-0113385, and the Office of Naval Research under grant N00014-01-1-0825.

receiver, respectively. The channel matrix can be described via the array steering and response vectors given by

$$\begin{aligned} \boldsymbol{a}_T(\theta_T) &= \frac{1}{\sqrt{P}}\left[1,\ e^{-j2\pi\theta_T},\cdots,e^{-j2\pi(P-1)\theta_T}\right]^T \\ \boldsymbol{a}_R(\theta_R) &= \frac{1}{\sqrt{Q}}\left[1,\ e^{-j2\pi\theta_R},\cdots,e^{-j2\pi(Q-1)\theta_R}\right]^T \end{aligned} \quad (2)$$

where θ is related to the AoA/AoD variable φ (measured with respect to the horizontal axis — see Figure 1) as $\theta = d\sin(\varphi)/\lambda = \alpha\sin(\varphi)$, λ is the wavelength of propagation, and $\alpha = d/\lambda$ is the normalized antenna spacing. We restrict ourselves to critical $(\lambda/2)$ spacing: $\alpha_T = \alpha_R = 0.5$. In this case, there is a one-to-one mapping between $\theta \in [-0.5, 0.5]$ and $\varphi \in [-\pi/2, \pi/2]$. The effect of larger antenna spacings is discussed in detail in [1].

The channel matrix $\boldsymbol{H}(t,f)$ can be generally modeled as

$$\boldsymbol{H}(t,f) = \sum_{n=1}^{N} \beta_n \boldsymbol{a}_R(\theta_{R,n})\boldsymbol{a}_T^H(\theta_{T,n})e^{j2\pi\nu_n t}e^{-j2\pi\tau_n f} \quad (3)$$

which corresponds to N propagation paths, $\{\theta_{T,n} \in [S_{T_-}, S_{T_+}] \subset [-0.5, 0.5)\}$ and $\{\theta_{R,n} \in [S_{R_-}, S_{R_+}] \subset [-0.5, 0.5)\}$ represent the spatial angles (AoDs/AoAs) seen by the transmitter and receiver, respectively, $\{\nu_n \in [-\nu_{\rm DS}, \nu_{\rm DS}]\}$ and $\{\tau_n \in [0, \tau_{\rm DS}]\}$ are the Doppler shifts and delays, respectively, and $\{\beta_n\}$ are the independent complex Gaussian path gains. $\tau_{\rm DS}$ denotes the delay spread, $\nu_{\rm DS}$ denotes the one-sided Doppler spread, and $[S_{T_-}, S_{T_+}]$ and $[S_{R_-}, S_{R_+}]$ represent the angular spreads.

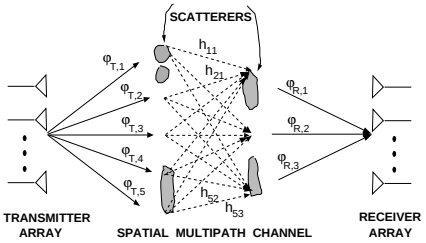

Fig. 1. *A schematic illustrating the* **virtual representation** *in the spatial dimension. The virtual angles are fixed a priori and their spacing defines the spatial resolution. The channel is characterized by the virtual coefficients,* $\{H_V(q,p) = h_{q,p}\}$*, that couple the* P *virtual transmit angles,* $\{\varphi_{T,p}\}$*, with the* Q *virtual receive angles,* $\{\varphi_{R,q}\}$*.*

3. VIRTUAL CHANNEL REPRESENTATION

In (3), each propagation path is associated with an AoD, AoA, delay and Doppler shift which can be arbitrarily distributed within the angular, delay and Doppler spreads. The virtual representation replaces the physical propagation paths with virtual ones corresponding to fixed AoD's, AoA's, delays and Doppler shifts that are determined by the spatial, temporal and spectral resolution afforded by the finite dimensional space-time signal space. The notion of virtual angles is illustrated in Figure 1. The *virtual channel representation* can be expressed as

$$\begin{aligned} \boldsymbol{H}(t,f) &= \sum_{q,p,m,l} H_V(q,p;m,l)\boldsymbol{a}_R(q/Q)\boldsymbol{a}_T^H(p/P) \\ &\quad e^{j2\pi mt/T}e^{-j2\pi lf/W} \end{aligned} \quad (4)$$

corresponding to fixed virtual AoD's, AoA's, delays and Doppler shifts defined as

$$\tilde{\theta}_{T,p} = \frac{p}{P},\ P_- \le p \le P_+, \quad \tilde{\theta}_{R,q} = \frac{q}{Q},\ Q_- \le q \le Q_+ \quad (5)$$

$$\widetilde{\nu}_m = \frac{m}{T},\ -M \le m \le M, \quad \widetilde{\tau}_l = \frac{l}{W},\ 0 \le l \le L, \quad (6)$$

where $L = \lceil W\tau_{\rm DS}\rceil$ and $M = \lceil T\nu_{\rm DS}\rceil$ denote the normalized delay and Doppler spreads. $P_- = \lfloor S_{T_-}P\rfloor$, $P_+ = \lceil S_{T_+}P\rceil$, $Q_- = \lfloor S_{R_-}Q\rfloor$, and $Q_+ = \lceil S_{R_+}Q\rceil$ represent the normalized angular spreads. The virtual channel coefficients $\{H_V(q,p;m,l)\}$ characterize the virtual representation. The transmit/receive virtual angle spacings represent the spatial resolutions that are determined by the array apertures ($\Delta\theta_T = 1/P$ and $\Delta\theta_R = 1/Q$). The virtual Doppler and delay spacings correspond to the spectral and temporal resolutions and are determined by the signaling duration and bandwidth ($\Delta\nu = 1/T$ and $\Delta\tau = 1/W$).

We now address the computation of the virtual representation from $\boldsymbol{H}(t,f)$. Assume WLOG that P, Q are odd and define $\widetilde{P} = (P-1)/2$, $\widetilde{Q} = (Q-1)/2$. The representation (4) can be decoupled as

$$\boldsymbol{H}(t,f) = \widetilde{\boldsymbol{A}}_R\boldsymbol{H}_V(t,f)\widetilde{\boldsymbol{A}}_T^H \quad (7)$$

$$\widetilde{\boldsymbol{A}}_R = [\boldsymbol{a}_R(-\widetilde{Q}/Q),\cdots,\boldsymbol{a}_R(\widetilde{Q}/Q)]\ (Q\times Q)$$

$$\widetilde{\boldsymbol{A}}_T = [\boldsymbol{a}_T(-\widetilde{P}/P),\cdots,\boldsymbol{a}_T(\widetilde{P}/P)]\ (P\times P), \quad (8)$$

where $\widetilde{\boldsymbol{A}}_R$ and $\widetilde{\boldsymbol{A}}_T$ are discrete Fourier transform matrices, as evident from (2) and (5).[1] The matrix $\boldsymbol{H}_V(t,f)$ in (7) is the partial virtual representation with respect to space and can be computed by beamforming in the direction of virtual angles

$$\begin{aligned} \boldsymbol{H}_V(t,f) &= \widetilde{\boldsymbol{A}}_R^H\boldsymbol{H}(t,f)\widetilde{\boldsymbol{A}}_T \\ &= \sum_{l=0}^{L}\sum_{m=-M}^{M}\boldsymbol{H}_V(m,l)e^{j2\pi mt/T}e^{-j2\pi lf/W} \end{aligned} \quad (9)$$

where the second equality further decomposes $\boldsymbol{H}_V(t,f)$ into component matrices $\boldsymbol{H}_V(m,l)$ corresponding to fixed virtual Doppler shifts and delays, which can be computed from $\boldsymbol{H}_V(t,f)$ as

$$\boldsymbol{H}_V(m,l) = \frac{1}{TW}\int_0^T\int_{-W/2}^{W/2}\boldsymbol{H}_V(t,f)e^{-j2\pi mt/T}e^{j2\pi lf/W}dtdf. \quad (10)$$

The elements of $\boldsymbol{H}_V(m,l)$ are related to the physical model (3) as

$$\begin{aligned} H_V(q,p;m,l) &= \sum_n \beta_n f_Q(\theta_{R,n}-q/Q)f_P^*(\theta_{T,n}-p/P) \\ &\quad e^{-j\pi(m-\nu_nT)}\mathrm{sinc}(m-\nu_nT)\mathrm{sinc}(l-\tau_nW) \end{aligned} \quad (11)$$

were $\mathrm{sinc}(x) = \sin(\pi x)/(\pi x)$ and

$$f_Q(\theta) = \frac{1}{Q}\sum_{i=0}^{Q-1}e^{-j2\pi\theta i} = \frac{1}{Q}e^{-j2\pi\theta\bar{Q}}\frac{\sin(\pi Q\theta)}{\sin(\pi\theta)}. \quad (12)$$

We note that $f_Q(\theta_R)$, $f_P(\theta_T)$, $\mathrm{sinc}(T\nu)$ and $\mathrm{sinc}(W\tau)$ get peaky around the origin with increasing Q, P, T and W.

[1] Note that $\widetilde{\boldsymbol{A}}_R$ and $\widetilde{\boldsymbol{A}}_T$ contain all possible virtual angles, some of which lie outside the angular spreads. $H_V(q,p;m,l)$ will be approximately zero for those angles.

3.1. Virtual Path Partitioning

The virtual representation induces a partitioning of propagation paths that is very insightful in determining their contribution to capacity and diversity and to expose the dependencies between the temporal, spectral and spatial degrees of freedom in the channel. Define the following subsets of propagation paths

$$\begin{aligned} S_{T,p} &= \{n : (p-1/2)/P \le \theta_{T,n} < (p+1/2)/P\} \quad (13)\\ S_{R,q} &= \{n : (q-1/2)/Q \le \theta_{R,n} < (q+1/2)/Q\} \quad (14)\\ S_{\nu,m} &= \{n : (m-1/2)/T \le \nu_n < (m+1/2)/T\} \quad (15)\\ S_{\tau,l} &= \{n : (l-1/2)/W \le \tau_n < (l+1/2)/W\} \quad (16)\end{aligned}$$

corresponding to transmit spatial resolution, receive spatial resolution, spectral resolution, and temporal resolution. Note that

$$\begin{aligned}\bigcup_p S_{T,p} &= \bigcup_q S_{R,q} = \bigcup_m S_{\nu,m} = \bigcup_l S_{\tau,l}\\ &= \bigcup_{p,q,m,l} S_{T,p} \cap S_{R,q} \cap S_{\nu,m} \cap S_{\tau,l} = \{1,2,\cdots,N\}. \quad (17)\end{aligned}$$

Then, $\boldsymbol{H}(t,f)$ can be approximately expressed as

$$\begin{aligned}\boldsymbol{H}(t,f) &= \sum_{q,p,m,l}\left[\sum_{n\in S_{q,p,m,l}}\beta_n\right]\\ &\quad \boldsymbol{a}_R(q/Q)\boldsymbol{a}_T^H(p/P)e^{j2\pi mt/T}e^{-j2\pi lf/W} \quad (18)\end{aligned}$$

where $S_{q,p,m,l} = S_{T,p}\cap S_{R,q}\cap S_{\nu,m}\cap S_{\tau,l}$ and the virtual channel coefficients in (11) can be approximated as

$$H_V(q,p;m,l) \approx \sum_{n\in S_{q,p,m,l}}\beta_n. \quad (19)$$

Equation (19) states that $H_V(q,p;m,l)$ is determined by the sum of gains of all paths that lie in $S_{q,p,m,l}$. The approximations in (18) and (19) get more accurate with increasing P, Q, T and W.

3.2. Channel Statistics

One of the most important characteristics of the virtual representation is that $\{H_V(q,p;m,l)\}$ are approximately uncorrelated under the assumption of uncorrelated path gains: $\mathrm{E}[\beta_n\beta_{n'}^*] = \sigma_n^2\delta_{n-n'}$ where δ_n denotes the kronecker delta function and σ_n^2 is the power in each path. This observation is directly evident from (19)

$$\begin{aligned}&\mathrm{E}[H_V(q,p;m,l)H_V^*(q',p';m',l')] \approx\\ &\left[\sum_{n\in S_{q,p,m,l}}\sigma_n^2\right]\delta_{q-q'}\delta_{p-p'}\delta_{m-m'}\delta_{l-l'} \quad (20)\end{aligned}$$

but can also be inferred from (11). Thus, from (18) we have

$$\begin{aligned}R_H(\Delta i,\Delta k;\Delta t,\Delta f) &= \mathrm{E}[H(i,k;t,f)H^*(i',k';t',f')]\\ &\approx \sum_{q,p,m,l}\sigma_{q,p,m,l}^2 e^{-j2\pi q\Delta i/Q}e^{j2\pi p\Delta k/P}\\ &\quad e^{j2\pi m\Delta t/T}e^{-j2\pi l\Delta f/W} \quad (21)\end{aligned}$$

where $\Delta i = i-i'$, $\Delta k = k-k'$, $\Delta t = t-t'$, $\Delta f = f-f'$, and

$$\begin{aligned}\sigma_{q,p,m,l}^2 &= \mathrm{E}[|H_V(q,p;m,l)|^2]\\ &= \sum_n \sigma_n^2 |f_Q(\theta_{R,n}-q/Q)|^2 |f_P(\theta_{T,n}-p/P)|^2\\ &\quad |\mathrm{sinc}(m-\nu_nT)|^2|\mathrm{sinc}(l-W\tau_n)|^2 \quad (22)\\ &\approx \sum_{n\in S_{q,p,m,l}}\sigma_n^2 \quad (23)\end{aligned}$$

is the power in $H_V(q,p;m,l)$ and the approximation in (23) is due to virtual path partitioning. Relation (21) yields the insightful conclusion that under the assumption of uncorrelated path gains, $\boldsymbol{H}(t,f)$ is a segment of a 4D WSS process in the two spatial dimensions, time and frequency, and $\{H_V(q,p;m,l)\}$ are the corresponding uncorrelated spectral representation. Furthermore, (23) states that the power in $H_V(q,p;m,l)$ is equal to the sum of the powers in the paths that lie in $S_{q,p,m,l}$. We note that the extent of correlation in space, frequency and time is inversely proportional to the angular, delay and Doppler spreads, respectively.

4. DEPENDENCIES IN TIME, FREQUENCY AND SPACE

From (4) we may conclude that the total independent degrees of freedom in the space-time channel are

$$N_{ST} = (Q_+ - Q_- + 1)(P_+ - P_- + 1)(L+1)(2M+1) \quad (24)$$

where $(Q_+ - Q_- + 1)(P_+ - P_- + 1)$ represents the degrees of freedom in space and $(L+1)(2M+1)$ represents the degrees in time and frequency. However, this conclusion implicitly assumes that the degrees of freedom in space, time and frequency are independent. We now use the notion of virtual path partitioning to demonstrate fundamental dependencies between time, frequency and space that cause the essential degrees of freedom to be less than the upperbound in (24).

The dependencies between time, frequency and space are due to the fact that the delay and Doppler spreads are related to the angular spreads. For given (q,p), $H_V(q,p;m,l)$ is non-vanishing over (l,m) between

$$L_{-(q,p)} = \left\lfloor\left[\min_{S_{q,p}}\tau_n\right]W\right\rfloor,\ L_{+(q,p)} = \left\lceil\left[\max_{S_{q,p}}\tau_n\right]W\right\rceil \quad (25)$$

$$M_{-(q,p)} = \left\lfloor\left[\min_{S_{q,p}}\nu_n\right]T\right\rfloor,\ M_{+(q,p)} = \left\lceil\left[\max_{S_{q,p}}\nu_n\right]T\right\rceil \quad (26)$$

where $S_{q,p} = S_{R,q}\cap S_{T,p}$. Consequently, (4) can be refined to limit the ranges of l and m as a function of (q,p) as above to reflect the essential degrees of freedom in the channel

$$N_{ST,ess} = \sum_{q,p}\sum_{l=L_{-(q,p)}}^{L_{+(q,p)}}\sum_{m=M_{-(q,p)}}^{M_{+(q,p)}} \le N_{ST}. \quad (27)$$

Note that $N_{ST,ess} = N_{ST}$ in (24) if and only if $(L_+ - L_- + 1)(M_+ - M_- + 1) = (L+1)(2M+1)$ for all (q,p) which would seldom be true particularly for channels that are *underspread* ($\tau_{\mathrm{DS}}\nu_{\mathrm{DS}} \ll 1$). This is because time/frequency selectivity exhibited by $H_V(q,p;t,f)$ depends on the spatial resolution: higher resolutions would result in less selectivity whereas lower resolutions will result in higher selectivity. A SISO channel will exhibit maximum time/frequency selectivity.

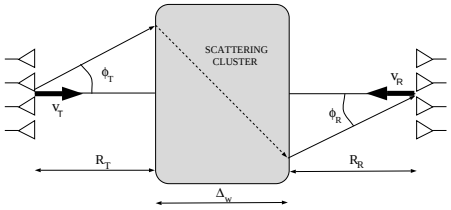

Fig. 2. *A schematic illustrating the dependence of delay and Doppler shift on the virtual transmit and receive angles.*

Figure 2 illustrates a simple scattering geometry to quantify such dependencies. Consider a single scattering cluster at a distance R_T from the transmitter and R_R from the receiver. Suppose that v_T denotes the relative speed between the transmitter and the cluster and v_R the relative speed between the receiver and the cluster. Let Δ_T and Δ_R denote the angular spreads, and Δ_w the "width" of the cluster. Via simple geometric considerations, τ and ν can be estimated for any given (θ_R, θ_T) as

$$\tau = \sqrt{\Delta_w^2 + |R_T\theta_T/\alpha_T - R_R\theta_R/\alpha_R|^2}/c \quad (28)$$

$$\nu = f_{\max,\mathrm{T}}\sqrt{1-{\theta_T}^2/\alpha_T^2} + f_{\max,\mathrm{R}}\sqrt{1-{\theta_R}^2/\alpha_R^2} \quad (29)$$

where c denotes the speed of light, $f_{\max,\mathrm{T}} = v_T/c$ and $f_{\max,\mathrm{R}} = v_R/c$. We note the expression for τ is stricly a lowerbound since multiple bounces [2] within the cluster may result in longer delays.

5. NUMERICAL RESULTS

We now present some numerical results to illustrate the effect of time/frequency selectivity on capacity and the effect of number of antennas on time/frequency selectivity of the channel. We simulated a single scattering cluster, as in Figure 2, with angular spreads of $\Delta_T = \Delta_R = 2\pi/3$ centered at $(\varphi_T, \varphi_R) = (0, 0)$. We considered $N = 100$ propagation paths. We first generated N pairs of angles, $\{\varphi_{R,n}, \varphi_{T,n}\}$, uniformly distributed within the angular spreads to fix the scatterer positions. To simulate time/frequency selectivity, we considered a temporal signal space with $N_o = TW = 65$ dimensions. We simulated three types of channels. **CH 1** (flat): $R_T = R_R = 1000$m, $f_{\max,\mathrm{R}} = f_{\max,\mathrm{T}} = 50$ Hz, $W = 1$ MHz, $T = 65\mu s$. **CH 2** (medium selective): $R = 8000$m, $f_{\max} = 400$ Hz, $W = 1$ MHz, $T = 65\mu s$. **CH 3** (highly selective): $R = 8000$m, $f_{\max} = 400$ Hz, $W = 10$ MHz, $T = 6.5\mu s$. $\Delta w = 100$m in all cases. Both **CH 1** and **CH 2** have the same T and W but **CH 2** has larger delay and Doppler spreads and is thus more selective. **CH 3** has the same delay and Doppler spreads but is even more selective than **CH 2** due to larger W (delay diversity is easier to exploit in this case). Channel realizations were generated using (3) via iid complex Gaussian $\{\beta_n\}$. Each realization was normalized to yield $\sum \beta_n^2 = PQ$.

Figure 3 illustrates the effect of time/frequency selectivity on outage capacity for $P = Q = 4$ antennas. The capacity was numerically computed using 200 independent channel realizations at an SNR of 20dB (details to be reported elsewhere). As evident, the outage capacity curves get steeper (higher diversity) as the channel gets more selective. The ergodic capacity of all three channels is approximately 21.8 bits/s/Hz. Note that this is consistent with the experimental results reported in [2] and in disagreement with analytical results reported in [3] which suggested that increased

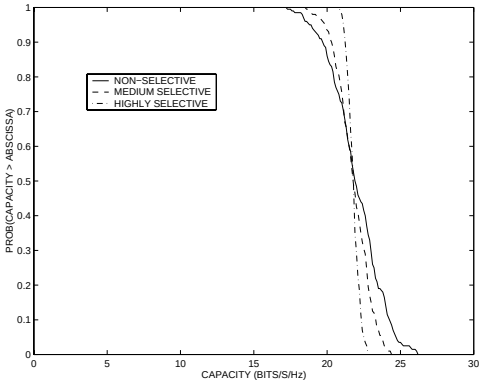

Fig. 3. *Comparison of the three channels illustrating the effect of time/frequency selectivity on outage capacity.*

delay spread can increase ergodic capacity. We can prove using our framework that frequency selectivity does not increase ergodic capacity and this apparent inconsistency with [3] is due to different modeling assumptions used in [3] (details to be reported elsewhere).

Figure 4 illustrates the dependencies between time, frequency and space. **CH 2** was simulated using $P = Q = 2$ and $P = Q = 4$ antennas. The figure shows contour plots of a subset of $\sigma^2_{q,p,m,l}$ as a function of (m, l) for a representative (q, p). It is evident that the delay-Doppler spread *decreases* in the virtual spatial domain for larger number of antennas, as predicted by our analysis. The number of significant $\sigma^2_{q,p,m,l}$ provides an estimate for $N_{ST,eff}$ in (27). Our simulations yielded $N_{ST,eff}/QP = 4.5$ in the 2-antenna case and 2.75 in the 4-antenna case, confirming that time/frequency selectivity decreases in the virtual spatial domain with increasing number of antennas.

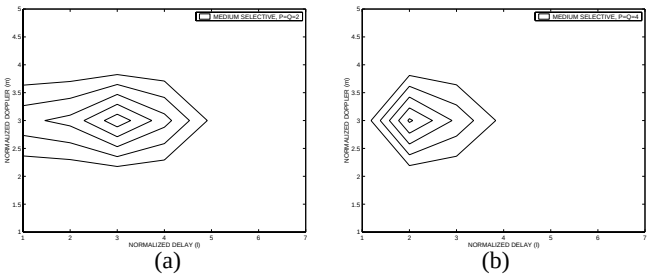

(a) (b)

Fig. 4. *Contour plots of the powers in a subset of non-vanishing virtual delay-Doppler coefficients for* **CH 2** *for a representative virtual angle pair* (q, p). *(a)* $Q = P = 2$. *(b)* $P = Q = 4$.

6. REFERENCES

[1] A. M. Sayeed, "Deconstructing multi-antenna fading channels," *IEEE Trans. Signal Processing*, pp. 2563-2579, Oct. 2002.

[2] A. F. Molisch, M. Steinbauer, M. Toeltsch, E. Bonek, and R. S. Thomä, "Capacity of MIMO systems based on measured wireless channels," *IEEE J. Selec. Areas. Commun.*, pp. 561–569, Apr. 2002.

[3] H. Bolcskei, D. Gesbert, and A. J. Paulraj, "On the capacity of OFDM-based spatial multiplexing systems," *IEEE Tran. Commun.*, pp. 225–234, Feb. 2002.